

First Measurement of the Tensor Structure Function b_1 of the Deuteron.

A. Airapetian,³¹ N. Akopov,³¹ Z. Akopov,³¹ M. Amarian,^{8,31} V.V. Ammosov,²³ A. Andrus,¹⁶ E.C. Aschenauer,⁸ W. Augustyniak,³⁰ R. Avakian,³¹ A. Avetissian,³¹ E. Avetissian,¹² P. Bailey,¹⁶ D. Balin,²² V. Baturin,²² M. Beckmann,⁷ S. Belostotski,²² S. Bernreuther,¹⁰ N. Bianchi,¹² H.P. Blok,^{21,29} H. Böttcher,⁸ A. Borissov,¹⁸ A. Borysenko,¹² M. Bouwhuis,¹⁶ J. Brack,⁶ A. Brüll,¹⁷ V. Bryzgalov,²³ G.P. Capitani,¹² T. Chen,⁴ H.C. Chiang,¹⁶ G. Ciullo,¹¹ M. Contalbrigo,¹¹ P.F. Dalpiaz,¹¹ R. De Leo,³ M. Demey,²¹ L. De Nardo,¹ E. De Sanctis,¹² E. Devitsin,¹⁹ P. Di Nezza,¹² J. Dreschler,²¹ M. Düren,¹⁴ M. Ehrenfried,¹⁰ A. Elalaoui-Moulay,² G. Elbakian,³¹ F. Ellinghaus,⁸ U. Elschenbroich,¹³ R. Fabbri,²¹ A. Fantoni,¹² A. Fechtchenko,⁹ L. Felawka,²⁷ B. Fox,⁶ S. Frullani,²⁵ G. Gapienko,²³ V. Gapienko,²³ F. Garibaldi,²⁵ K. Garrow,^{1,26} E. Garutti,²¹ D. Gaskell,⁶ G. Gavrilov,^{7,27} V. Gharibyan,³¹ G. Graw,²⁰ O. Grebeniounk,²² L.G. Greeniaus,^{1,27} I.M. Gregor,⁸ K. Hafidi,² M. Hartig,²⁷ D. Hasch,¹² D. Heesbeen,²¹ M. Henoeh,¹⁰ R. Hertenberger,²⁰ W.H.A. Hesselink,^{21,29} A. Hillenbrand,¹⁰ M. Hoek,¹⁴ Y. Holler,⁷ B. Hommez,¹³ G. Iarygin,⁹ A. Ivanilov,²³ A. Izotov,²² H.E. Jackson,² A. Jgoun,²² R. Kaiser,¹⁵ E. Kinney,⁶ A. Kisselev,²² M. Kopytin,⁸ V. Korotkov,²³ V. Kozlov,¹⁹ B. Krauss,¹⁰ V.G. Krivokhijine,⁹ L. Lagamba,³ L. Lapikás,²¹ A. Laziev,^{21,29} P. Lenisa,¹¹ P. Liebing,⁸ L.A. Linden-Levy,¹⁶ K. Lipka,⁸ W. Lorenzon,¹⁸ H. Lu,⁵ J. Lu,²⁷ S. Lu,¹⁴ B.-Q. Ma,⁴ B. Maiheu,¹³ N.C.R. Makins,¹⁶ Y. Mao,⁴ B. Marianski,³⁰ H. Marukyan,³¹ F. Masoli,¹¹ V. Mexner,²¹ N. Meyners,⁷ O. Mikloukho,²² C.A. Miller,^{1,27} Y. Miyachi,²⁸ V. Muccifora,¹² A. Nagaitsev,⁹ E. Nappi,³ Y. Naryshkin,²² A. Nass,¹⁰ M. Negodaev,⁸ W.-D. Nowak,⁸ K. Oganessyan,^{7,12} H. Ohsuga,²⁸ N. Pickert,¹⁰ S. Potashov,¹⁹ D.H. Potterveld,² M. Raithel,¹⁰ D. Reggiani,¹¹ P.E. Reimer,² A. Reischl,²¹ A.R. Reolon,¹² C. Riedl,¹⁰ K. Rith,¹⁰ G. Rosner,¹⁵ A. Rostomyan,³¹ L. Rubacek,¹⁴ J. Rubin,¹⁶ D. Ryckbosch,¹³ Y. Salomatin,²³ I. Sanjiev,^{2,22} I. Savin,⁹ A. Schäfer,²⁴ C. Schill,¹² G. Schnell,^{8,28} K.P. Schüller,⁷ J. Seele,¹⁶ R. Seidl,¹⁰ B. Seitz,¹⁴ R. Shanidze,¹⁰ C. Shearer,¹⁵ T.-A. Shibata,²⁸ V. Shutov,⁹ M.C. Simani,^{21,29} K. Sinram,⁷ M. Stancari,¹¹ M. Statera,¹¹ E. Steffens,¹⁰ J.J.M. Steijger,²¹ H. Stenzel,¹⁴ J. Stewart,⁸ F. Stinzinger,¹⁰ U. Stösslein,⁶ P. Tait,¹⁰ H. Tanaka,²⁸ S. Taroian,³¹ B. Tchuiko,²³ A. Terkulov,¹⁹ A. Tkabladze,¹³ A. Trzcinski,³⁰ M. Tytgat,¹³ A. Vandenbroucke,¹³ P. van der Nat,^{21,29} G. van der Steenhoven,²¹ M.C. Vetterli,^{26,27} V. Vikhrov,²² M.G. Vincter,¹ C. Vogel,¹⁰ M. Vogt,¹⁰ J. Volmer,⁸ C. Weiskopf,¹⁰ J. Wendland,^{26,27} J. Wilbert,¹⁰ Y. Ye,⁵ Z. Ye,⁷ S. Yen,²⁷ B. Zihlmann,²¹ and P. Zupranski³⁰

(The HERMES Collaboration)

¹Department of Physics, University of Alberta, Edmonton, Alberta T6G 2J1, Canada

²Physics Division, Argonne National Laboratory, Argonne, Illinois 60439-4843, USA

³Istituto Nazionale di Fisica Nucleare, Sezione di Bari, 70124 Bari, Italy

⁴School of Physics, Peking University, Beijing 100871, China

⁵Department of Modern Physics, University of Science and Technology of China, Hefei, Anhui 230026, China

⁶Nuclear Physics Laboratory, University of Colorado, Boulder, Colorado 80309-0446, USA

⁷DESY, 22603 Hamburg, Germany

⁸DESY, 15738 Zeuthen, Germany

⁹Joint Institute for Nuclear Research, 141980 Dubna, Russia

¹⁰Physikalisches Institut, Universität Erlangen-Nürnberg, 91058 Erlangen, Germany

¹¹Istituto Nazionale di Fisica Nucleare, Sezione di Ferrara and

Dipartimento di Fisica, Università di Ferrara, 44100 Ferrara, Italy

¹²Istituto Nazionale di Fisica Nucleare, Laboratori Nazionali di Frascati, 00044 Frascati, Italy

¹³Department of Subatomic and Radiation Physics, University of Gent, 9000 Gent, Belgium

¹⁴Physikalisches Institut, Universität Gießen, 35392 Gießen, Germany

¹⁵Department of Physics and Astronomy, University of Glasgow, Glasgow G12 8QQ, United Kingdom

¹⁶Department of Physics, University of Illinois, Urbana, Illinois 61801-3080, USA

¹⁷Laboratory for Nuclear Science, Massachusetts Institute of Technology, Cambridge, Massachusetts 02139, USA

¹⁸Randall Laboratory of Physics, University of Michigan, Ann Arbor, Michigan 48109-1120, USA

¹⁹Lebedev Physical Institute, 117924 Moscow, Russia

²⁰Sektion Physik, Universität München, 85748 Garching, Germany

²¹Nationaal Instituut voor Kernfysica en Hoge-Energiefysica (NIKHEF), 1009 DB Amsterdam, The Netherlands

²²Petersburg Nuclear Physics Institute, St. Petersburg, Gatchina, 188350 Russia

²³Institute for High Energy Physics, Protvino, Moscow region, 142281 Russia

²⁴Institut für Theoretische Physik, Universität Regensburg, 93040 Regensburg, Germany

²⁵Istituto Nazionale di Fisica Nucleare, Sezione Roma 1, Gruppo Sanità
and Physics Laboratory, Istituto Superiore di Sanità, 00161 Roma, Italy

²⁶Department of Physics, Simon Fraser University, Burnaby, British Columbia V5A 1S6, Canada

²⁷TRIUMF, Vancouver, British Columbia V6T 2A3, Canada

²⁸Department of Physics, Tokyo Institute of Technology, Tokyo 152, Japan

²⁹Department of Physics and Astronomy, Vrije Universiteit, 1081 HV Amsterdam, The Netherlands

³⁰Andrzej Soltan Institute for Nuclear Studies, 00-689 Warsaw, Poland

³¹Yerevan Physics Institute, 375036 Yerevan, Armenia

(Dated: February 8, 2020)

The HERMES experiment has investigated the tensor spin structure of the deuteron using the 27.6 GeV/c positron beam of HERA. The use of a tensor polarized deuteron gas target with only a negligible residual vector polarization enabled the first measurement of the tensor asymmetry A_{zz}^d and the tensor structure function b_1^d for average values of the Björken variable $0.01 < \langle x \rangle < 0.45$ and of the squared four-momentum transfer $0.5 \text{ GeV}^2 < \langle Q^2 \rangle < 5 \text{ GeV}^2$. The quantities A_{zz}^d and b_1^d are found to be non-zero. The rise of b_1^d for decreasing values of x can be interpreted to originate from the same mechanism that leads to nuclear shadowing in unpolarized scattering.

PACS numbers: 13.60.-r, 13.88.+e, 14.20.Dh, 14.65.-q

Inclusive deep-inelastic scattering (DIS) of charged leptons from the deuteron, a spin-1 object, is described by eight structure functions, twice as many as required to describe DIS from a spin-1/2 nucleon [1]. The three leading-twist structure functions relevant to this discussion can be written within the Quark-Parton Model as [1]:

	Nucleon	Deuteron
F_1	$\frac{1}{2} \sum_q e_q^2 [q_\uparrow^{\frac{1}{2}} + q_\uparrow^{-\frac{1}{2}}]$	$\frac{1}{3} \sum_q e_q^2 [q_\uparrow^1 + q_\uparrow^{-1} + q_\uparrow^0]$
g_1	$\frac{1}{2} \sum_q e_q^2 [q_\uparrow^{\frac{1}{2}} - q_\downarrow^{\frac{1}{2}}]$	$\frac{1}{2} \sum_q e_q^2 [q_\uparrow^1 - q_\downarrow^1]$
b_1	--	$\frac{1}{2} \sum_q e_q^2 [2q_\uparrow^0 - (q_\uparrow^1 + q_\uparrow^{-1})]$

where q_\uparrow^m (q_\downarrow^m) is the number density of quarks with spin up(down) along the z axis in a hadron(nucleus) with helicity m moving with infinite momentum along the z axis. Reflection symmetry implies that $q_\uparrow^m = q_\downarrow^{-m}$. The sums run over quark and antiquark flavors q with a charge e_q in units of the elementary charge e . Both structure functions and quark number densities depend on the Björken variable x which can be interpreted as the fraction of the nucleon momentum carried by the struck quark in the infinite-momentum frame, and $-Q^2$, the square of the four-momentum transfer by the virtual photon.

The polarization-averaged structure function F_1 describes the quark distributions averaged over the target spin states. The polarization-dependent structure function g_1 describes the imbalance in the distribution of quarks with the same (q_\uparrow^m) or opposite (q_\downarrow^m) helicity with respect to that of the parent hadron. It can be measured only when both beam and target are polarized. The tensor structure function b_1 does not exist for spin-1/2 targets. It describes the difference in the quark distributions between the helicity-0 $q^0 = (q_\uparrow^0 + q_\downarrow^0) = 2q_\uparrow^0$ and the averaged non-zero helicity $q^1 = (q_\uparrow^1 + q_\downarrow^1) = (q_\uparrow^1 + q_\uparrow^{-1})$ states of the deuteron [1, 2, 3]. Because b_1 depends only on the spin averaged quark distributions $b_1 = \frac{1}{2} (q^0 - q^1)$, its measurement does not require a polarized beam. The tensor structure function b_1^d vanishes in the absence of nuclear effects, i.e. if the deuteron simply consists of a

proton and neutron in a relative S -state [1]. Since the magnitude of b_1^d was expected to be small, it was usually ignored in the extraction of the deuteron structure function g_1^d and, as a consequence, of the neutron structure function g_1^n derived from deuteron and proton data. This is in general not *a priori* justified. This paper reports the first measurement of b_1^d , performed by the HERMES collaboration using a data set taken with a positron beam and a tensor-polarized deuterium target, and an integrated luminosity of 24 pb^{-1} .

The HERMES experiment [4] was designed to investigate the internal spin structure of nucleons and nuclei by deep-inelastic scattering of polarized positrons and electrons by polarized gaseous targets (e.g. hydrogen, deuterium and helium-3) internal to the HERA- e storage ring. The positrons (electrons) circulating in the ring become transversely polarized by the emission of spin-flip synchrotron radiation [5]. A longitudinal beam polarization is generated at HERMES by the use of a pair of spin rotators before and after the experiment. Beam polarization is employed for the simultaneous g_1^d measurement and for studies on beam related systematic effects on b_1^d .

A feature of HERMES unique among polarized DIS experiments is its atomic-gas target that is not diluted by non-polarizable material [6]. The target cell is an open-ended elliptical aluminum tube internal to the beam line (40 cm long, 75 μm in wall thickness and $21 \times 9 \text{ mm}^2$ in cross section), which is used to confine the polarized gas along the beam. A magnetic field surrounding the target and aligned with the beam provides the quantization axis for the nuclear spin. A sample of gas was continuously drawn from the cell and analyzed to determine the atomic and molecular abundances and the nuclear polarization of the atoms. The deuterium atom has a total of six hyperfine states defined by the relative orientation of the electron and nuclear spins. An atomic beam source (ABS) generates a deuterium atomic beam and selects the two hyperfine states with the desired nuclear polarization to be injected into the target cell. This system allows the selection of substates with pure tensor polarization P_{zz} and at the same time vanishing vector polarization P_z , a combination which is not possible for solid-state po-

TABLE I: Hyperfine state composition of target injection modes [6], corresponding atomic populations, and ideal (100%) polarizations inside the target cell.

Injection mode	Hyperfine state composition	Atomic population	Ideal target pol.	
			Vector	Tensor
vector ⁺	$ 1\rangle + 6\rangle$	n^+	1	1
vector ⁻	$ 3\rangle + 4\rangle$	n^-	-1	1
tensor ⁺	$ 3\rangle + 6\rangle$	$n^+ + n^-$	0	1
tensor ⁻	$ 2\rangle + 5\rangle$	n^0	0	-2

larized targets. Every 90 seconds the polarization of the injected gas is changed; for the b_1^d measurement the four injection modes listed in Tab. I were continuously cycled. The vector and tensor atomic polarizations of the target are defined as

$$P_z = \frac{n^+ - n^-}{n^+ + n^- + n^0}, \quad P_{zz} = \frac{n^+ + n^- - 2n^0}{n^+ + n^- + n^0}, \quad (1)$$

where n^+ , n^- , n^0 are the atomic populations with positive, negative and zero spin projection on the beam direction, respectively. In order to maximize the statistical accuracy, the analysis described below uses the four independent injection modes of the target to compare the DIS yields for tensor⁻ mode ($P_{zz} < 0$) with the averaged yields of the vector⁺, vector⁻ and tensor⁺ modes ($P_{zz} > 0$). Note that the vector⁺ and vector⁻ modes are also employed for the g_1^d measurement.

The HERMES detector [4] is a forward spectrometer with a dipole magnet providing a field integral of 1.3 Tm. A horizontal iron plate shields the HERA beam lines from this field, thus dividing the spectrometer into two identical halves with ± 170 mrad horizontal and ± 40 to ± 140 mrad vertical acceptance for the polar scattering angle. In this analysis, a set of criteria was implemented to define accurately the effective active area of the spectrometer. Tracking is based on 36 drift chamber planes in each detector-half. Positron identification is accomplished using a likelihood method based on signals of four subsystems: a ring-imaging Čerenkov detector, a lead-glass calorimeter, a transition-radiation detector, and a preshower hodoscope. For positrons in the momentum range of 2.5 to 27 GeV/c, the identification efficiency exceeds 98% and the hadron contamination is less than 0.5%. The average polar angle resolution is 0.6 mrad and the average momentum resolution is 2%.

For a target state characterized by P_z and P_{zz} , the DIS yield measured by the experiment is proportional to the double differential cross section of polarized DIS

$$\frac{d^2\sigma_P}{dx dQ^2} \simeq \frac{d^2\sigma}{dx dQ^2} \left[1 - P_z P_B D A_1^d + \frac{1}{2} P_{zz} A_{zz}^d \right]. \quad (2)$$

Here, σ is the unpolarized cross section, A_1^d is the vector and A_{zz}^d the tensor asymmetry of the virtual-photon deuteron cross section, P_B is the beam polarization and D is the fraction of the beam polarization transferred

TABLE II: Polarizations of the target states employed in the b_1^d measurement as described in the text. The average beam polarization $|P_B|$ is 0.53 ± 0.01 . The average target vector P_z and tensor P_{zz} polarizations are typically more than 80% of the ideal values listed in Tab. I. A residual vector polarization not more than 0.01 is achieved both for the σ^0 , σ^{\leftrightarrow} and the averaged $(\sigma^{\vec{\leftarrow}} + \sigma^{\vec{\rightarrow}})/2$ measurements.

measured yield	vector term	tensor term
	$P_z \cdot P_B$	P_{zz}
$\sigma^{\vec{\rightarrow}}$	$+0.45 \pm 0.02$	$+0.80 \pm 0.03$
$\sigma^{\vec{\leftarrow}}$	-0.45 ± 0.02	$+0.85 \pm 0.03$
σ^{\leftrightarrow}	0.00 ± 0.01	$+0.89 \pm 0.03$
σ^0	0.00 ± 0.01	-1.65 ± 0.05

to the virtual photon. In Eq. 2 and in the following Eq. 4, the fractional correction ($\lesssim 0.01$) arising from the interference between longitudinal and transverse photoabsorption amplitudes, which leads to the structure function g_2 [7], is neglected. Four independent polarized yields were measured (see Tab. II for the values of the achieved polarizations): $\sigma^{\vec{\rightarrow}}$ and $\sigma^{\vec{\leftarrow}}$ when the target spin is parallel and anti-parallel to that of the beam, respectively, σ^{\leftrightarrow} when the target has a mixture of helicity-1 states, and σ^0 when the target is in the helicity-0 state. The tensor asymmetry is extracted as

$$A_{zz}^d = \frac{2\sigma^1 - 2\sigma^0}{3\sigma_U P_{zz}^{\text{eff}}}, \quad (3)$$

where $\sigma^1 = (\sigma^{\vec{\leftarrow}} + \sigma^{\vec{\rightarrow}} + \sigma^{\leftrightarrow})/3$ is the average over the helicity-1 states, $\sigma_U = (2\sigma^1 + \sigma^0)/3$ is the polarization-averaged yield and $P_{zz}^{\text{eff}} = (P_{zz}^{\vec{\rightarrow}} + P_{zz}^{\vec{\leftarrow}} + P_{zz}^{\leftrightarrow} - 3P_{zz}^0)/9$ is the effective tensor polarization. In Eq. 3 the vector component due to A_1^d nearly cancels out (see Tab. II). Note that any contribution from residual vector polarization of the target is reduced to a negligible level by grouping together two sets of data with approximately the same statistics and opposite beam helicities.

The polarization-dependent structure function g_1^d can be extracted from the vector asymmetry A_1^d as

$$\frac{g_1^d}{F_1^d} \simeq A_1^d \simeq \frac{c_{zz}}{|P_z P_B| D} \frac{(\sigma^{\vec{\leftarrow}} - \sigma^{\vec{\rightarrow}})}{(\sigma^{\vec{\leftarrow}} + \sigma^{\vec{\rightarrow}})}, \quad (4)$$

$$\text{with } c_{zz} = \frac{(\sigma^{\vec{\leftarrow}} + \sigma^{\vec{\rightarrow}})}{2\sigma_U} = 1 + \frac{(P_{zz}^{\vec{\rightarrow}} + P_{zz}^{\vec{\leftarrow}})}{4} A_{zz}^d. \quad (5)$$

In all previous determinations of g_1^d the contribution of the tensor asymmetry A_{zz}^d was neglected, i.e. c_{zz} was assumed to be equal to 1, in spite of the fact that the vector polarization of the target could only be generated together with a non-zero tensor polarization. The present measurement quantifies the effect of A_{zz}^d on the existing g_1^d data.

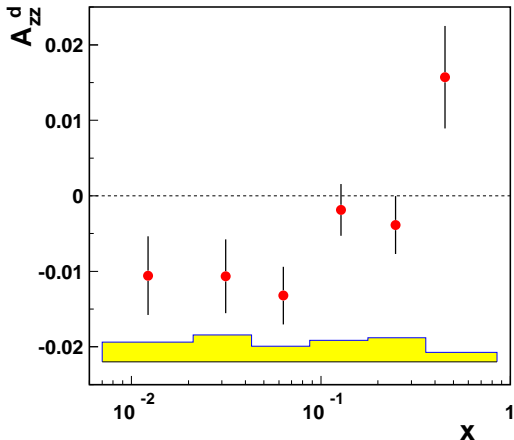


FIG. 1: The tensor asymmetry $A_{zz}^d(x)$. The error bars are statistical and the shaded band shows the systematic uncertainty.

For the determination of A_{zz}^d , about 2.4 million inclusive events obtained with a tensor-polarized deuterium target are selected, by requiring as in the HERMES g_1^d analysis [8] a scattered positron with $0.1 \text{ GeV}^2 < Q^2 < 20 \text{ GeV}^2$ and an invariant mass of the virtual-photon nucleon system $W > 1.8 \text{ GeV}$. The kinematic range covered by the selected data is $0.002 < x < 0.85$ and $0.1 < y < 0.91$, where y is the fraction of the beam energy carried by the virtual photon in the target rest frame. The asymmetry A_{zz}^d is calculated according to Eq. 3. The number of events determined per spin state is corrected for the e^+e^- background arising from charge symmetric processes (the latter is negligible at high x but amounts to almost 15% of the statistics in the low- x bin) and normalized to the luminosity measured by Bhabha scattering from the target gas electrons [4].

The asymmetry A_{zz}^d is corrected for detector smearing and QED radiative effects to obtain the Born asymmetry corresponding to pure single-photon exchange in the scattering process. The radiative corrections are calculated using a Monte Carlo generator based on RADGEN [9]. The kinematic migration of the events due to radiative and detector smearing is treated using an unfolding algorithm, which is only sensitive to the detector model, the known unpolarized cross section, and the models for the background processes [10]. The coherent and quasi-elastic radiative tails are estimated using parameterizations of the deuteron form factors [11, 12] and corrected for the tracking inefficiency due to showering of the radiated photons. The polarized part of the quasi-elastic radiative tail is neglected since there is no net tensor effect by inclusive scattering on weakly-bound spin-1/2 objects [13]. The extracted tensor asymmetry A_{zz}^d is shown in Fig. 1 and listed in Tab. III. It appears to be positive at high x and is negative at low x , crossing zero at an x value of about 0.2. The magnitude of the observed tensor asymmetry A_{zz}^d does not exceed 0.02 over the measured

TABLE III: Measured values of the tensor asymmetry A_{zz}^d and the tensor structure function b_1^d . Both the corresponding statistical and systematic uncertainties are listed as well.

$\langle x \rangle$	$\langle Q^2 \rangle$ GeV ²	A_{zz}^d $\times 10^{-2}$	$\delta A_{zz}^{\text{stat}}$ $\times 10^{-2}$	$\delta A_{zz}^{\text{sys}}$ $\times 10^{-2}$	b_1^d $\times 10^{-2}$	δb_1^{stat} $\times 10^{-2}$	δb_1^{sys} $\times 10^{-2}$
0.012	0.51	-1.06	0.52	0.26	11.20	5.51	2.77
0.032	1.06	-1.07	0.49	0.36	5.50	2.53	1.84
0.063	1.65	-1.32	0.38	0.21	3.82	1.11	0.60
0.128	2.33	-0.19	0.34	0.29	0.29	0.53	0.44
0.248	3.11	-0.39	0.39	0.32	0.29	0.28	0.24
0.452	4.69	1.57	0.68	0.13	-0.38	0.16	0.03

range; from this result and using Eqs. 4 and 5, the fractional correction to the HERMES g_1^d measurement due to the tensor asymmetry is estimated to be less than 0.01.

The particle identification efficiency, the target polarization measurement and the luminosity measurement (sensitive to possible residual polarization of the target gas electrons) give negligible contributions to the systematic uncertainty. The normalization uncertainty between different injection modes of the ABS is $\approx 1 \times 10^{-3}$ and correlated over the kinematic bins. This uncertainty is estimated by the observed 2-sigma offset from zero of the asymmetry between averaged vector ($2\sigma^1 = \sigma^{\vec{\sigma}} + \sigma^{\vec{\sigma}^{\perp}}$) and tensor⁺ (σ^0 replaced by σ^{\leftrightarrow} in Eq. 3) non-zero helicity injection modes. The subtraction of the radiative background inflates the size of the statistical and the above mentioned systematic uncertainties by almost a factor of 2 at low x . The systematic uncertainty of the radiative corrections is $\approx 2 \times 10^{-3}$ for the three bins at low x and negligible at high x . A possible misalignment in the spectrometer geometry yields an uncertainty $\approx 3 \times 10^{-3}$ in the bins where the asymmetry changes sign. All the contributions to the systematic uncertainty are added in quadrature. The two subsamples of data with opposite beam helicities were analyzed independently and gave consistent A_{zz}^d results.

The tensor structure function b_1^d is extracted from the tensor asymmetry using the relations [18, 28]

$$b_1^d = -\frac{3}{2} A_{zz}^d F_1^d ; \quad F_1^d = \frac{(1 + \gamma^2) F_2^d}{2x(1 + R)}. \quad (6)$$

No contribution from the hitherto unmeasured double spin-flip structure function Δ [14] is considered here, being kinematically suppressed for a longitudinally polarized target [15]. The structure function F_2^d is calculated as $F_2^d = F_2^p(1 + F_2^n/F_2^p)/2$ using the parameterizations of the precisely measured structure function F_2^p [16] and F_2^n/F_2^p ratio [17]. In Eq. (6), $R = \sigma_L/\sigma_T$ is the ratio of longitudinal to transverse photo-absorption cross sections [18] and $\gamma = \sqrt{Q^2}/\nu$ is a kinematic factor (ν being the virtual-photon energy). The results for b_1^d are listed together with those for A_{zz}^d in Tab. III. The behavior of b_1^d is displayed in Fig. 2. The data show that b_1^d is different from zero, its magnitude rises for decreasing values

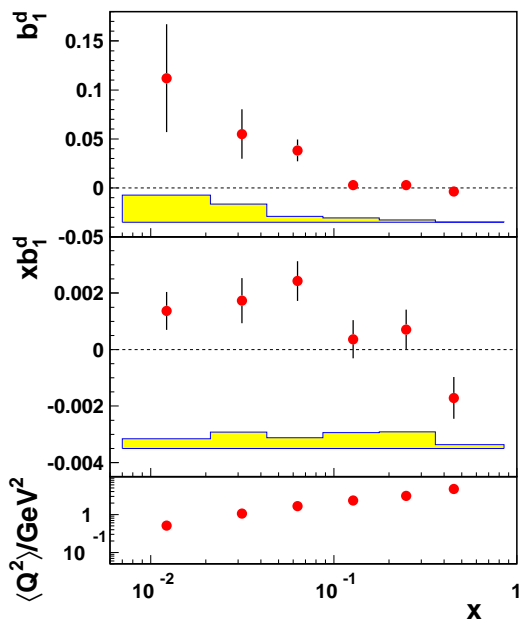


FIG. 2: The tensor structure function presented as (top) $b_1^d(x)$ and (middle) $x b_1^d(x)$. The error bars are statistical and the shaded bands show the systematic uncertainty. The bottom panel shows the average value of Q^2 in each x -bin.

of x and, for $x \lesssim 0.03$, becomes even larger than that of g_1^d at the same value of Q^2 [8, 19].

Because the deuteron is a weakly-bound state of spin-1/2 nucleons, b_1^d was initially predicted to be negligible, at least at moderate and large values of x ($x > 0.2$) [20, 21, 22], where it should be driven by nuclear binding and Fermi motion effects. It was later realized that significant contributions to b_1^d at $x < 0.1$ could be generated by the same mechanism that leads to the well known effect of nuclear shadowing in unpolarized scattering [23]. This feature is described by coherent double-scattering models [24, 25, 26, 27, 28, 29]. The first investigation of double-scattering contributions to polarization-dependent deuteron structure functions was performed in Ref. [24] neglecting the D -state component. With its inclusion, it was found that b_1^d could rise to values different from zero as $x \rightarrow 0$, and its magnitude could reach about 1% of the unpolarized structure function F_1^d [25, 26, 27, 28, 29]. The observed b_1^d confirms qualitatively the double-scattering model predictions, except for the negative value at $\langle x \rangle = 0.452$, which, however, is still compatible with zero on the 2 sigma level. In the context of the Quark-Parton Model description, the sum rule $\int b_1(x) dx = 0$ is broken if the quark sea is tensor polarized [30, 31]. As can be seen from Fig. 2, the first moment of b_1^d is not zero within the measured range: $\int_{0.002}^{0.85} b_1(x) dx$ is calculated to be $(1.05 \pm 0.34_{\text{stat}} \pm 0.35_{\text{sys}}) \cdot 10^{-2}$ at $Q^2 = 5 \text{ GeV}^2$, if b_1^d and F_1^d are assumed to have the same Q^2 dependence. Within the restricted x -range where $Q^2 > 1 \text{ GeV}^2$, $\int_{0.02}^{0.85} b_1(x) dx$

is calculated to be $(0.35 \pm 0.10_{\text{stat}} \pm 0.18_{\text{sys}}) \cdot 10^{-2}$ at $Q^2 = 5 \text{ GeV}^2$.

In conclusion, HERMES has provided the first measurement of the tensor structure function b_1^d , in the kinematic domain $0.01 < \langle x \rangle < 0.45$ and $0.5 \text{ GeV}^2 < \langle Q^2 \rangle < 5 \text{ GeV}^2$. The function b_1^d and its first moment are found to be different from zero within the measured x range. The b_1^d measurement can be used to reduce the systematic uncertainty on the g_1^d measurement that is assigned to the tensor structure of the deuteron. The behavior of b_1^d at low values of x is in qualitative agreement with expectations based on coherent double-scattering models.

We gratefully acknowledge the DESY management for its support, the staff at DESY and the collaborating institutions for their significant effort, and our funding agencies for financial support. We are grateful to N. Nikolaev and O. Shekhovtsova for useful discussions.

-
- [1] P. Hoodbhoy *et al.*, Nucl. Phys. B **312**, 571 (1989).
 - [2] A. Pais, Phys. Rev. Lett. **19**, 544 (1967).
 - [3] L. L. Frankfurt *et al.*, Nucl. Phys. A **405**, 557 (1983).
 - [4] HERMES Coll., K. Ackerstaff *et al.*, Nucl. Instr. Meth. A **417**, 230 (1998).
 - [5] A. Sokolov and L. Ternov, Sov. Phys. Doklady **8**, 1203 (1964).
 - [6] HERMES Coll., A. Airapetian *et al.*, Nucl. Instr. Meth. A **540**, 68 (2005).
 - [7] E155 Coll., P. L. Anthony *et al.*, Phys. Lett. B **553**, 18 (2003).
 - [8] HERMES Coll., g_1 paper, in preparation. C. Riedl, in *Proc. of 16th International Spin Physics Symposium*, Trieste 2004, hep-ex/0411087.
 - [9] I. V. Akushevich *et al.*, hep-ph/9906408.
 - [10] HERMES Coll., A. Airapetian *et al.*, Phys. Rev. D **71**, 012003 (2005).
 - [11] D. Abbott *et al.*, Eur. Phys. J. A **7**, 421 (2000).
 - [12] S. Stein *et al.*, Phys. Rev. **12**, 1884 (1975).
 - [13] Z.-L. Zhou *et al.*, Phys. Rev. Lett. **82**, 687 (1999).
 - [14] R. L. Jaffe *et al.*, Phys. Lett. B **223**, 218 (1989).
 - [15] E. Sather *et al.*, Phys. Rev. D **42**, 1424 (1990).
 - [16] H. Abramowicz *et al.*, hep-ph/9712415.
 - [17] NMC, P. Amaudruz *et al.*, Nucl. Phys. B **371**, 3 (1992).
 - [18] L. W. Whitlow *et al.*, Phys. Lett. B **250**, 193 (1990).
 - [19] C. Riedl, PhD-thesis, in preparation.
 - [20] G. A. Miller, in *Electronuclear Physics with Internal Targets*, ed. R. G. Arnold (World Scientific, Singapore, 1989), p.30.
 - [21] H. Khan *et al.*, Phys. Rev. C **44**, 1219 (1991).
 - [22] A. Yu. Umnikov, Phys. Lett. B **391**, 177 (1997).
 - [23] EMC, J. Ashman *et al.*, Phys. Lett. B **206**, 364 (1988).
 - [24] H. Khan *et al.*, Phys. Lett. B **298**, 181 (1993).
 - [25] M. Strikman, in *Proceedings of the Symposium on Spin Structure of the Nucleon*, ed. V. H. Hughes and C. Cavata (World Scientific, Singapore, 1995), p.153.
 - [26] N. N. Nikolaev *et al.*, Phys. Lett. B **398**, 245 (1997).
 - [27] J. Edelmann *et al.*, Z. Phys. A **357**, 129 (1997).
 - [28] J. Edelmann *et al.*, Phys. Rev. C **57**, 3392 (1998).
 - [29] K. Bora *et al.*, Phys. Rev. D **57**, 6906 (1998).
 - [30] F. E. Close *et al.*, Phys. Rev. D **42**, 2377 (1990).

[31] A. V. Efremov *et al.*, Sov. J. Nucl. Phys. **36**, 557 (1982).